Clustering under short-range finite interactions

M. Tirado-Miranda,[1] A. Schmitt,[2] J. Callejas-Fernández,[2] and A. Fernández-Barbero[3,*]
[1]*Department of Physics, University of Extremadura, 10071 Cáceres, Spain*
[2]*Biocolloid and Fluid Physics Group, Department of Applied Physics, University of Granada, 18071 Granada, Spain*
[3]*Complex Fluid Physics Group, Department of Applied Physics, University of Almería, 04120 Almería, Spain*
(Received 17 May 2002; published 21 January 2003)

In this paper the aggregation of surface modified colloidal particles is presented, paying special attention to the cluster structure and growth. The surface was modified by adsorbing bovine serum albumin (BSA). The interaction potential develops a minimum of restricted depth, weakening the clusters which subsequently restructure and form more compact morphologies. This minimum is responsible for the reversibility of the aggregation processes (this is an important difference between diffusion-limited cluster aggregation and reaction-limited cluster aggregation). The energy minimum is associated with the presence of a steric term in the energy balance, which depends on the size of the adsorbed molecules. BSA molecules with different sizes were employed to test this point. In addition, the short-range interaction seems not to affect significantly the paths of approximating particles, since the aggregation of the clusters at long times is independent of the size of these particles. The long-time kinetics was interpreted in the frame of dynamic scaling concepts. A kinetics model, including surface-surface, protein-surface, and protein-protein aggregation, is used to determine the dominant mechanism controlling the aggregation.

DOI: 10.1103/PhysRevE.67.011402 PACS number(s): 61.43.Hv, 82.70.Dd, 83.80.Hj

INTRODUCTION

It is well known that irreversible colloidal particle aggregation leads to clusters exhibiting fractal structures directly related to the aggregation mechanism. For noninteracting particles, the movement is dominated by the interaction with the solvent molecules, undergoing Brownian diffusion only affected by particle correlations induced by hydrodynamic interactions. This interaction reduces the aggregation rate by a factor two with regard to that of pure Brownian motion. Aggregation dominated by this mechanism is characterized by a linear increase of the mean cluster mass with the time. Moreover, the free particle paths lead to a fractal cluster with fractal dimension ~ 1.8.

When repulsion stabilizing longe-ranged forces dominate, the cluster mass initially grows exponentially with time and later crosses over to power law growth with an exponent greater than one. Furthermore, the mean-square displacement decreases. The repulsion allows the colliding particles to reach positions interior to the cluster arms, making the clusters more compact with fractal dimensions ~ 2.1. These two limit regimes describing irreversible processes are usually called diffusion-limited cluster aggregation (DLCA) and reaction-limited cluster aggregation (RLCA), respectively. These two regimes, as well as the crossover between them, have been widely studied during the past two decades [1–4].

A topical subject deals with modifications on clustering induced by the presence of a short-range barrier between particles. It can be achieved by irreversible adsorption of macromolecules onto the particle surfaces [5–7]. The aim of the current paper is to yield new insights on the mechanism governing the kinetics and cluster structure when those short-range interactions are dominant. Thus, static light scattering (SLS) and dynamic light scattering were used to study the cluster structure and the evolution of the mean cluster mass, respectively. Bovine serum albumin (BSA) was employed as an adsorbed macromolecule, since its charge state is easily controlled through the pH of the medium. In order to study the effect of that short-range interaction on the cluster structure, a high salt concentration was employed for the experiments, thus screening the long-range electrostatic repulsive interaction, which assures us that the morphological modifications should be related only to the short-range interaction.

After the macromolecules are adsorbed, the interaction potential develops a minimum of restricted depth, weakening the clusters which subsequently restructure and form more compact morphologies. Moreover, this minimum is responsible for the reversibility of the aggregation processes (this is an important difference with DLCA and RLCA). The energy minimum is associated with the presence of a steric term in the energy balance, which depends on the size of the adsorbed molecules. BSA molecules with different sizes were employed in order to test this point. In addition, the short-range interaction seems not to affect significantly the paths of approximating particles, and the aggregation of the clusters at long times was found to be independent of the size of these particles. The long-time kinetics data were interpreted by using dynamic scaling concepts [8,9].

Three aggregation mechanisms have been considered in the present paper to explain the experimental results at short aggregation times. (i) Surface-surface aggregation: the aggregation between bare sites on the particle surfaces must be dominant for low molecule concentration. (ii) Protein-surface aggregation: free parts of the absorbed molecules, oriented towards the bulk of the solution, are able to adsorb also on the surface of colliding particles, (when free sites are available), giving rise to bridging aggregation [5,10]. (iii) Protein-protein aggregation: the interaction between mol-

*Corresponding author. Email address: afernand@ual.es

ecules on different particles can also originate an additional aggregation. In addition, the steric barrier could impede particle aggregation, when enough protein is adsorbed.

The outline of this paper is as follows: Section I is a theoretical background, including a brief summary about static and dynamic light scattering applied to colloidal aggregation. Section II describes the experimental systems. Section III contains the experimental details. The results and the discussion of these experimental details are presented in Sec. IV.

I. THEORETICAL BACKGROUND

A. Scattering functions for fractal structures

Colloidal clusters show self-similar branched structures characterized by a scaling law, $V(R) \sim R^{d_f}$, which relates the increasing radius R to the cluster volume $V(R)$ through the fractal dimension d_f. Static light scattering (SLS) allows the cluster fractal dimension, d_f, to be determined from the angular dependence of the mean scattered intensity. For elastic scattering, the scattered light intensity from a system of clusters may be expressed in a factorized form as [11]

$$I(q) \sim P(q) S(q), \tag{1}$$

where $q = 4\pi/\lambda \sin(\theta/2)$ is the scattering wave vector, with λ being the wavelength of the light in the solvent and θ the scattering angle. The form factor, $P(q)$, is related to the particle size and shape. The structure factor, $S(q)$, depends on the relative positions of the particles within the clusters and hence contains the information about the structure. This factor is essentially a Fourier transform of the pair correlation function $g(r)$,

$$S(q) \sim \int r^2 [g(r) - 1] \frac{\sin(qr)}{qr} dr. \tag{2}$$

In the case of fractal structures growing in three-dimensional space, the pair correlation function is related to the fractal dimension $g(r) \sim r^{d_f - 3}$. Equation (2) is integrated, leading to [12]:

$$S(q) \sim \Gamma(d_f - 1) \frac{\sin[(d_f - 1)\arctan(qR)]}{qR[1 + (qR)^2]^{(d_f - 1)/2}} \sim q^{-d_f} \quad (qR \gg 1), \tag{3}$$

where R is the mean aggregate size. Thus, in the $qR \gg 1$ limit, a power law in the scattering vector is expected, from which the fractal dimension may be determined. The structure factor is defined only for distances larger than the particle size and thus, Eq. (3) is only valid for $qR_0 < 1$, where R_0 is the monomer size. In this scattering region, the influence of the particle form factor can be neglected and the angular variation of the intensity is related only to the cluster structure factor [$I(q) \sim q^{-d_f}$]. For higher q values, the length scale corresponds to individual spheres within the cluster and the intensity is related to the particle form factor. In lower-q regions, topological length correlations between clusters could be studied.

B. Monitoring of cluster growth

The aggregation kinetics for colloidal suspensions is described by the time evolution of the cluster size distribution $N_n(t)$. For dilute systems, where only binary collisions are relevant, von Smoluchowski proposed the following differential equations: $dN_n/dt = \frac{1}{2}\Sigma_{i+j=n} k_{ij} N_i N_j - N_n \Sigma_{k=1}^{\infty} k_{nk} N_k$ [13]. The function k_{ij} is the rate at which i-mers bind to j-mers. That function depends on the sizes of the colliding clusters and contains all the physical information. For DLCA, all collisions are effective (a short-range attractive force is needed to guarantee bond irreversibility). The aggregation is then called diffusion controlled. This is the fastest possible aggregation mode in the absence of attraction forces between particles.

1. Long-time behavior

Most coagulation kernels used in literature are homogeneous functions of i and j, at least for large i and j. Van Dongen and Ernst [8] introduced a classification scheme for these type of kernels, $k_{ai,aj} \propto a^{\lambda} k_{ij}$, where a is a positive constant. The homogeneity parameter λ describes the tendency of a large cluster to bind to another large cluster and governs the overall rate of aggregation. It should take the value 0 for DLCA and 1 for RLCA. λ will be used in the current paper to characterize the aggregation mechanism. λ may be determined from the evolution of the number average mean cluster size, $\langle n_n \rangle = M_1/M_0$, where $M_i = \Sigma n^i N_n$ is the i-order moment of the size distribution. For DLCA a linear increase with time is expected for long aggregation times, $\lim_{t \to \infty} \langle n_n \rangle(t) \sim t$. In the case of RLCA an exponential behavior is predicted, $\lim_{t \to \infty} \langle n_n \rangle(t) \sim e^{\alpha t}$, where α is a fitting constant. In an intermediate regimen where the aggregation is not totally controlled by diffusion or repulsion, the number average mean cluster size, for nongelling systems ($0 \leqslant \lambda < 1$), increases describing a power law in time with the exponent related to the homogeneity parameter:

$$\lim_{t \to \infty} \langle n_n \rangle(t) \sim t^{1/(1-\lambda)}. \tag{4}$$

The mean mass for fractal clusters may be derived from the mean hydrodynamic radius, $\langle R_h \rangle(t)$, once the fractal dimension is known and from this magnitude, the number-average mean cluster size is easily calculated by dividing the mean cluster mass by the monomer mass [14],

$$\langle n_n \rangle = \frac{\langle M \rangle}{m_0} = \left(\frac{\langle R_h \rangle}{R_0} \right)^{d_f}, \tag{5}$$

with m_0 and R_0 being the monomer mass and radius, respectively. This equation is employed in the present paper to obtain λ. DLS is employed to determine the mean cluster size, $\langle R_h \rangle$. The scattered intensity autocorrelation function is determined directly from the photomultiplier output and converted into the scattered field autocorrelation function using the Siegert relationship [15]. Information on the cluster-size distribution is obtained from the fitting coefficient in the expanded logarithm of the field autocorrelation function (cumulant analysis), $\ln g^{\text{field}}(\tau) = -\mu_1 \tau + \mu_2(\tau^2/2) + \mu_3(\tau^3/3!)$

$+\cdots$. The first cumulant μ_1 is related to the mean particle diffusion coefficient by $\mu_1=\langle D\rangle q^2$. Once the mean diffusion coefficient is determined, the mean hydrodynamic size may be calculated using the Stokes-Einstein relationship. The homogeneity exponent, λ, is then obtained from the long-time asymptotic behavior of the mean cluster size, according to Eq. (4).

2. Short-time behavior

Olivier and Sorensen [16] obtained the following equation for the first cummulant of the intensity autocorrelation function, valid for shorter times:

$$\mu_1(t)=\mu_1(0)\left(1+\frac{t}{t_c}\right)^{-1/d_f(1-\lambda)}, \tag{6}$$

where $t_c=2/c_0k_s$ is the characteristic aggregation time. It is expressed as a function of the initial particle concentration c_0 and the Smoluchowski rate constant, k_s. Equation (6) allows the characteristic aggregation time, t_c, to be obtained, once d_f and λ are known. After that, k_s is determined from t_c using the initial particle concentration. This method is valid due to the fact that both the fractal structure and the dynamic scaling become apparent almost since the beginning of the aggregation processes [7,17].

II. EXPERIMENTAL SYSTEMS

A. Polystyrene particles

Aqueous suspensions of surfactant stabilized polystyrene microspheres (MA80) were used for the aggregation experiments. The particle diameter and polydispersity were determined by transmission electron microscopy (TEM) as well as by photocorrelation spectroscopy (PCS). The number average mean particle size ($\langle d_n\rangle=M_1/M_0$ with $M_k=\Sigma_k n_i d_i^k$) was determined to be $\langle d_n\rangle_{\mathrm{TEM}}=(99\pm4)$ nm and $\langle d_n\rangle_{\mathrm{PCS}}=(100\pm9)$. The system polydispersity was calculated by considering also the weigh average mean particle size. The polydispersity index from TEM was calculated using $\Delta_{\mathrm{TEM}}=\langle d_p\rangle/\langle d_n\rangle=M_4M_0/M_3M_1$ to be (1.006 ± 0.005). For the PCS measurements, the polydispersity index was calculated from the first and second cumulants, $\Delta_{\mathrm{PCS}}=\mu_2/\mu_1^2$ to be (0.04 ± 0.01). The negative surface charge responsible for the system stability arises from sulphate groups. Conductimetric titrations were performed in order to determine the total surface charge. In addition, charging and discharging potentiometric titrations were carried out to obtain the charge pH dependence. The surface charge density at pH=4.8 (set for the aggregation experiments) was (-2.5 ± 0.1) μC/cm^2. The particle stability was estimated by determining the critical coagulation concentration (CCC) equal to (0.50 ± 0.07) M from the time evolution of the mean scattered intensity.

B. Protein molecules

Bovine serum albumin (BSA) was chosen as an adsorbed macromolecule. This globular protein with molecular weight 66411 g mol^{-1} and 11.6 nm×2.7 nm×2.7 nm has the ability to form covalent dimers through the SH group in its polypeptidic chains. In this paper, monomeric (BSA-*m*) and polymeric (BSA-*p*) proteins were employed as a way of modifying the steric repulsive interaction potential. This protein presents the advantage that the charge can be balanced from negative to positive by a simple pH change around 4.8 the (BSA isoelectric point). Moreover, this protein shows low structural stability which imply structural changes. This fact leads to more stable unions which guarantees irreversible adsorption under well established conditions.

The protein suspensions were cleaned by dialysis against distilled and deionized water during three days till water conductivity remained constant. Afterwards, a Millipore 0.2 μm low affinity filter was employed. The protein concentration was calculated from the absorbance peak at 280 nm length wave using a spectrophotometer Spectronic-601, Milton Roy. The specific adsorption at that length wave is 0.667 1 g^{-1} m^{-1}. The concentrations were 4.25 mg/ml and 4.04 mg/ml for the monomeric and polymeric proteins, respectively.

In order to determine the protein sample composition, electrophoresis in polyacrilamide gel with silver dyeing was employed. Thus, the sample BSA-*m* is mainly composed of monomers with the presence of a very reduced band corresponding to dimers. However, the sample BSA-*p* is mainly composed of dimmers with a trace amount of monomer detected.

The amount of adsorbed protein was determined from adsorption isotherms, measured using a volume of 5 ml over 0.4 m^2 of total adsorption surface. Acetate buffers with a pH=4.8, corresponding to the BSA isoelectric point, were employed in order to guarantee maximum protein adsorption [18,19]. Polystyrene particles added to a protein solution were incubated during 2 h at 25 °C. The amount of nonadsorbed protein was determined from absorbance measurements after centrifugation and filtration using low affinity filters. Figure 1 shows the adsorption isoterms corresponding to monomeric and polymeric BSA. The added protein is adsorbed onto the particle surfaces until a monolayer is formed. Beyond this breakpoint, the slope becomes less tilted and the excess of added protein stays in the bulk solution. The values pointed out in the plot as 25%, 50%, 75%, and 100% correspond to the systems used in the aggregation experiments.

III. EXPERIMENT DETAILS

Aggregation starts after mixing equal amounts of sample and buffered electrolyte by means of a Y-shaped mixing device. Samples with different degrees of surface coverage were aggregated at high electrolyte concentration (0.700 M). The pH was set close to the isoelectric point of BSA (pH =4.8) for which the protein is globally discharged. The initial particle concentration was 1.6×10^{10} cm^{-3} and the temperature was stabilized at (25 ± 1) °C.

Simultaneous static and dynamic light-scattering experiments were performed using a 4700 Malvern setup. The mean scattered intensity was recorded in the range 10°–150°, showing an asymptotic time-independent behavior when the final structure of the clusters is totally established.

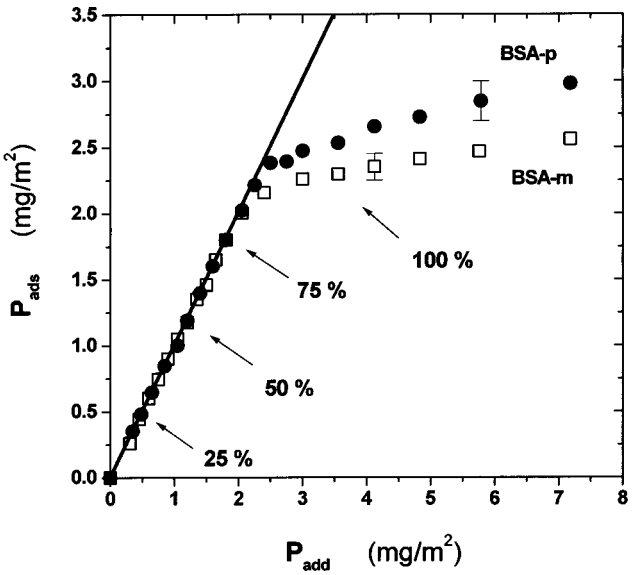

FIG. 1. Adsorption isoterms for the monomeric and polymeric proteins, where P_{add} and P_{ads} represent the amount of protein added and adsorbed, respectively. The arrow-marked points correspond to the systems employed in the aggregation experiments. For 100% surface coverage, the excess of protein in the bulk was cleaned before aggregation. In order to keep the experimental conditions unaltered, the same procedure was applied to all the samples although it would not be strictly necessary because of total protein adsorption.

From this long-time limit curve, the fractal dimensions were calculated. The number average mean cluster-size and the aggregation rate constant for dimer formation were determined from dynamic light scattering using Eqs. (5) and (6), respectively.

IV. RESULTS AND DISCUSSION

A. Aggregation of bare particles

Before the aggregation experiments with surface modified particles, bare polystyrene microspheres were coagulated under well-known conditions, i.e., under pure particle diffusion and under the presence of repulsive coulombian interactions, for which KCl was added at a concentration in the range 0.125–0.700 M. Using SLS, decreasing long-time asymptotic power laws were obtained for the mean scattering intensities, indicating a regular fractal structure (Fig. 2). The fractal dimensions are plotted in the inset, as a function of the salt concentration, observing a crossover from 1.75, for diffusion conditions to 2.1, when the interaction between particles is especially relevant. These values are commonly accepted in the literature for DLCA and RLCA, respectively. The average particle size, $\langle R_h \rangle$, was measured by DLS as a function of the ionic concentration. Using the fractal dimensions and the mean particle size, the number average mean cluster size was obtained and plotted in Fig. 3. The homogeneity parameter λ (inset in Fig. 3) was calculated from the exponent of the long-time scaling power law [Eq. (4)]. The time evolution also follows the expected behavior when crossing from DLCA to RLCA. At high salt concentration,

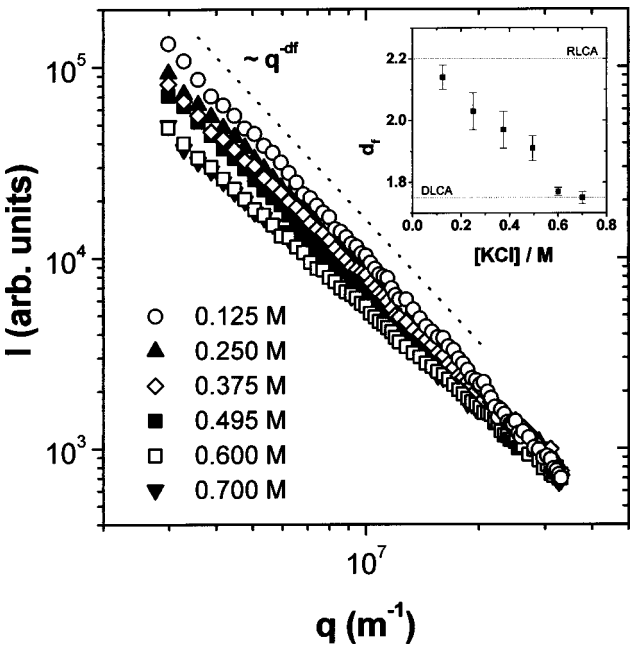

FIG. 2. Scattered intensity for bare particles aggregating under the presence of different ionic concentrations. From the exponents of the power laws, the fractal dimensions are calculated (inset).

$\lambda \approx 0$, describing a size independent cluster activity, typical for DLCA. However, when energy barriers are present, larger aggregates are more active than smaller ones and λ increases. In the literature there exist a wide range of values for λ in the range 0–1; this fact is associated with the experimental difficulty of establishing the repulsion-controlled aggregation limit [14,20,21].

B. Aggregation of surface modified particles

Aggregates were formed from monomers with different amounts of adsorbed BSA. In order to modify the range of

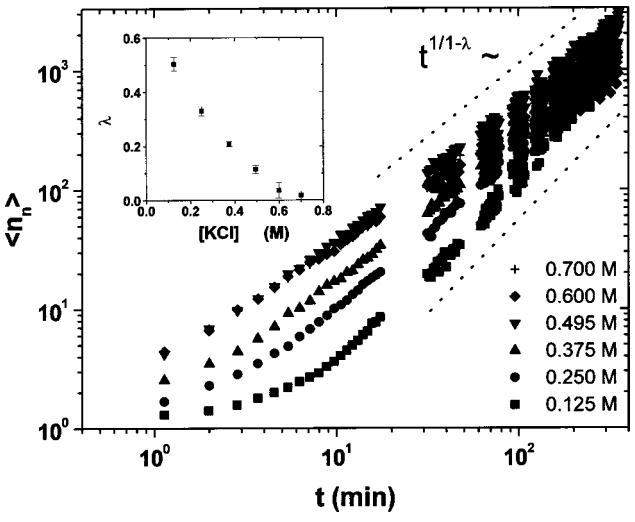

FIG. 3. Evolution of the number average cluster size during the aggregations. Different runs correspond to different ionic concentrations. The long-time asymptotic slopes contain kinetics information through the λ parameter, which is plotted in the upper left-hand corner as a function of salt concentration.

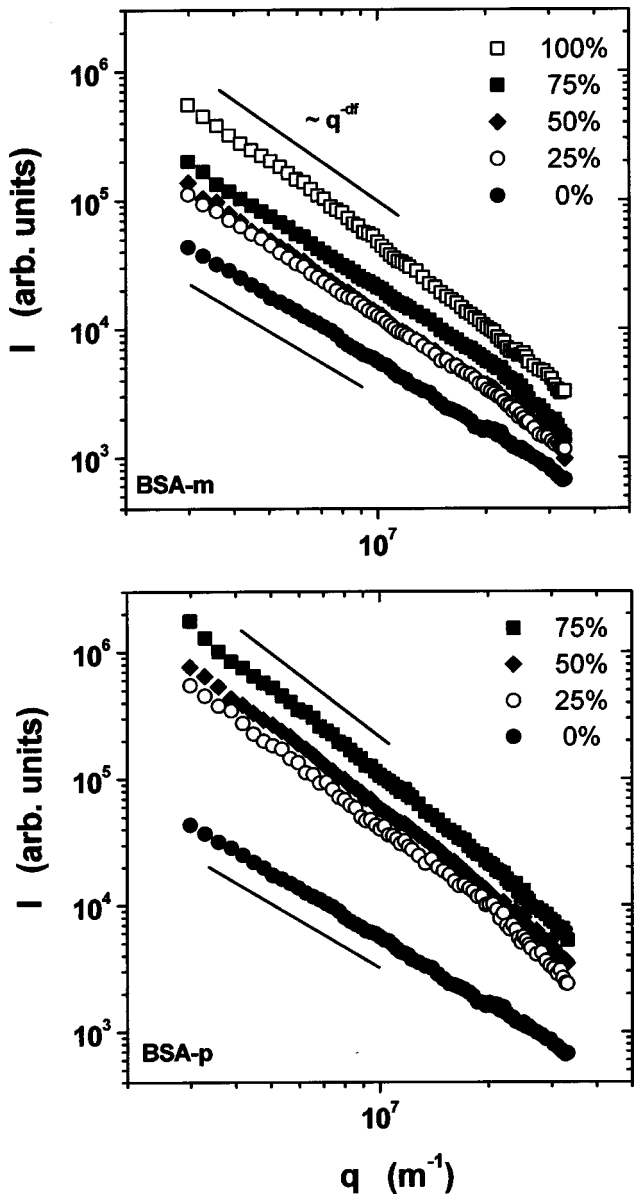

FIG. 4. Scattered light intensity against the transfer scattering moment corresponding to aggregating particles covered with different amounts of monomeric and polymeric protein (BSA-*m* and BSA-*p*).

the repulsive barrier responsible for the finite minimum in the interaction energy, monomeric (BSA-*m*) and polymeric (BSA-*p*) protein molecules were employed.

1. Cluster structure

Figure 4 plots the mean intensity spectrum as a function of the scattering angle for clustering with BSA-*m* and BSA-*p*. Decreasing power laws are exhibited for all protein coverages, indicating a regular fractal structure. In Fig. 5 the fractal dimensions are plotted against the degree of protein coverage. For the BSA-*m* the variation of the slopes with the amount of added protein is much less relevant than for BSA-*p*. The fractal dimension starts growing from 1.75 corresponding to DLCA. It is raised slightly for increasing adsorbed BSA-*m* till 75% of coverage, indicating that the cluster structure became more compact. For even more added protein, the fractal dimension increases dramatically reaching a value 2.1. This experiment was repeated three times to ensure the validity of this result. For BSA-*p*, the increase in the fractal dimension was much more pronounced. The cluster fractal dimension increases up to 2.1 for 25% coverage. Above this surface coverage, very compact clusters form with a fractal dimension in the range of that typical for RLCA. Vincent *et al.* [22] found that adsorbed polyelectrolytes strongly influence the colloidal aggregation due to important steric effects. A steric repulsive potential should then be added to the classical DLVO contributions for a proper description, i.e., the Coulombic repulsive potential and the London–van der Waals attractive potential. A new force balance has to be considered: now, not only the electrostatic force but also the steric force competes against the van der Waals attractive force, resulting in a strong repulsion barrier at very short distances, which impedes tight unions. The osmotic repulsive potential is expressed as

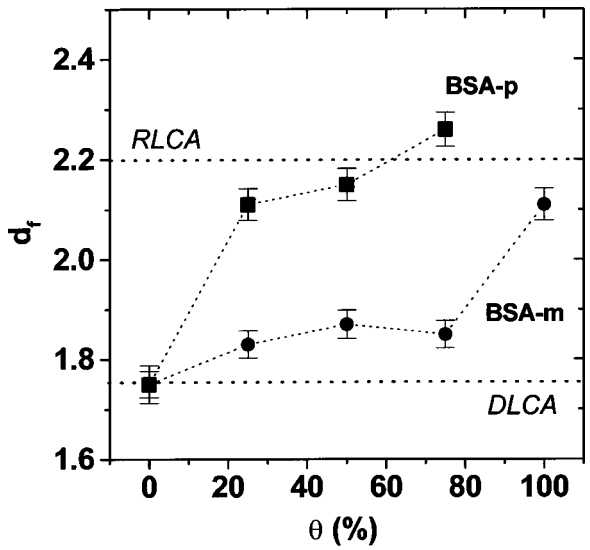

FIG. 5. Influence of the protein surface coverage on the fractal dimension of growing clusters. The two series correspond to monomeric and polymeric adsorbed protein.

$$V_{\mathrm{osm}}=\frac{4\pi a}{\nu}\phi^2\left(\frac{1}{2}-\chi\right)\delta^2\left[\left(\frac{H}{2\delta}\right)-\frac{1}{4}-\ln\left(\frac{H}{\delta}\right)\right], \qquad (7)$$

where δ is the distance between the particle surfaces due to the presence of adsorbed layers, ν is the molecular volume of the solvent, ϕ is the effective volume fraction of molecules in the adsorbed layer, and χ is the solvency parameter. The osmotic term dominates over the rest of the contributions when the particle surfaces are closer than a distance δ, producing a minimum becoming deeper as the separation between particles is reduced. Figure 6 shows the potential energy versus distance. The clusters formed at this finite minimum interaction potential present a weaker internal structure as compared with those growing under the van der Waals interaction. Thus, monomer rearrangement within the clusters is possible.

For BSA-*m*, the fractal dimensions are larger in the presence of the protein molecules. For values of the minimum on

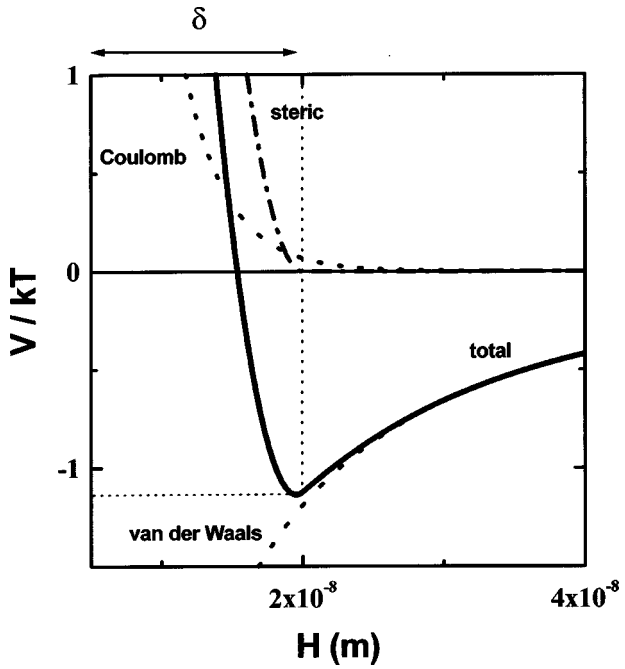

FIG. 6. Free energy for two particles under the presence of repulsive Coulombic interaction, van der Waals attraction, and steric repulsion due to adsorbed macromolecules. The total interaction energy (solid line) is obtained by adding up the three terms. It shows a finite minimum responsible for the weak attraction forces which make possible monomer rearrangement within the clusters. In the absence of steric interaction, the minimum disappears since the cluster structure is controlled only by the strength of the repulsive Coulombic interaction.

the order of k_BT, the thermal energy controls the cluster structure, provoking particle rearrangement. The potential energy minimum becomes less pronounced as the distance δ increases. As illustrated in Fig. 7, at low coverage degree, the distance between particle surfaces is very short and cluster structures are close to that corresponding to DLCA. For higher surface coverage the fractal dimension increases as a consequence of particle separation. The large rise of the fractal dimension at 100% of coverage degree could be related to the fact that protein might be adsorbed with an end-side orientation. The mean separation between particles should be larger, and the energy minimum less marked, favoring monomer rearrangement.

The fractal dimensions for BSA-*p* covered particles follows basically the same trend observed with BSA-*m*. However, the fractal dimensions are much larger which corresponds to more compact structures. The presence of polymeric protein makes separation δ larger. In addition, the effective volume fraction of molecules in the adsorbed layer ϕ also increases. The solvency parameter χ is constant since the nature of the adsorbed molecules and the solvent do not change (the dependence of χ on the volume fraction necessary to explain phase transitions in some types of polymer gels is considered insignificant in the present model). Consequently, the steric potential (7) increases as well as its range for polymeric adsorbed protein as compared with the monomeric one. The potential energy minimum (Fig. 6) re-

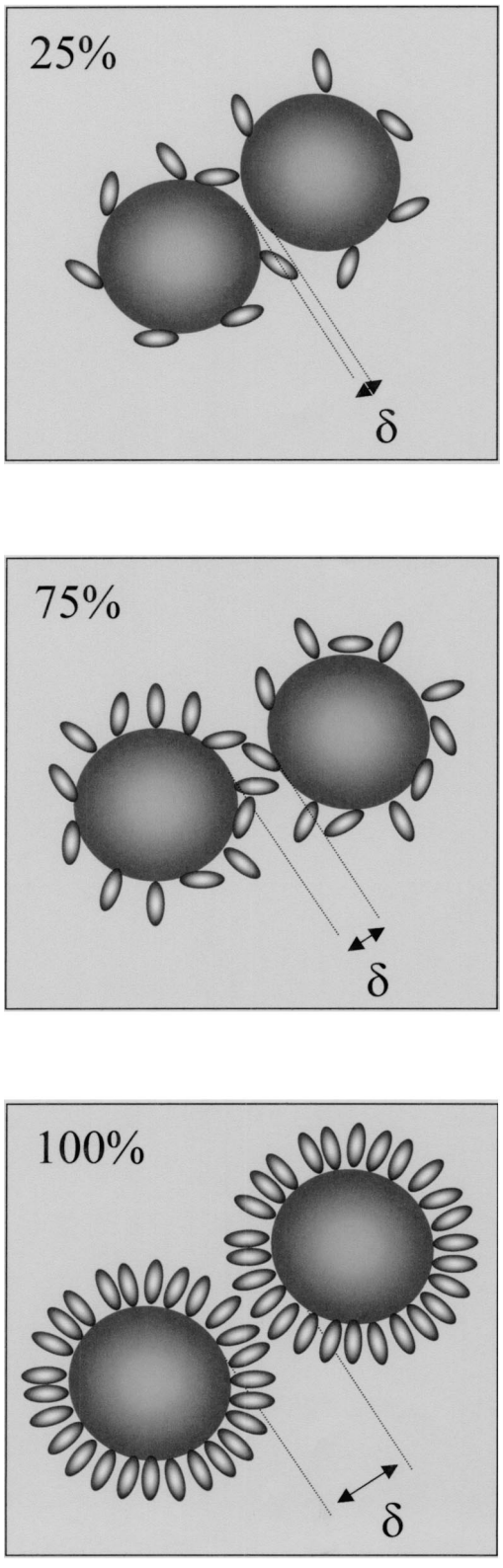

FIG. 7. Sketch to illustrate the increase of the monomer separation into clusters for increasing surface coverage. The strong fractal dimension rise observed in Fig. 5 at 100% of surface coverage (for BSA-*m*) could be related to the fact that protein molecules adsorbed in a very compact configuration as shown in the picture.

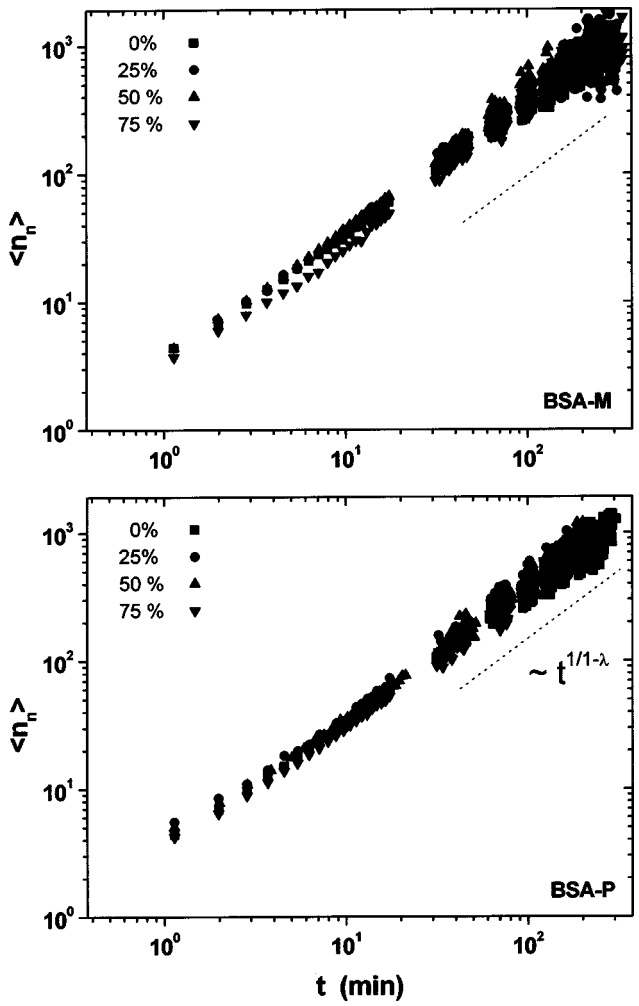

FIG. 8. Number average cluster size for clusters growing under different amounts of adsorbed protein (BSA-*m* and BSA-*p*). From the slopes at long time, the λ parameter is obtained and plotted in Fig. 9.

duces its depth, shifting towards larger distances. Therefore, the cluster restructuring is favored by the presence of larger steric separations.

2. Aggregation kinetics

The aggregation kinetics at long times was monitored by dynamic light scattering. The number-average mean cluster size was calculated from the mean hydrodynamic radius and fractal dimension [Eq. (5)]. In this way, variations on the clustering mechanism might be detected from the asymptotic long-time scaling behavior. Figure 8 plots $\langle n_n \rangle$ as a function time for different coverage with BSA-*m* and BSA-*p*. All curves exhibit the predicted power law in the time with very similar evolutions. The values of λ were calculated from the exponents (Fig. 9). They are close to 0 showing a slight rise for increasing surface coverage. Clusters are then formed mainly after a pure diffusion process (DLCA). This result is expected since the BSA molecules modify only the interaction between the particles at short distances, not affecting the particle paths. In fact, no significant changes are observed for

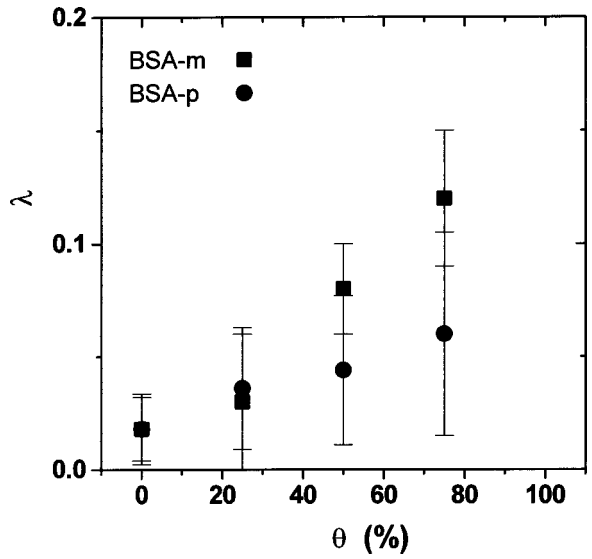

FIG. 9. Kinetics λ parameter for different surface coverage degrees. A regular slight increase is shown as the coverage increases.

polymeric adsorbed protein compared to the monomeric one, despite the steric barrier shifts to larger distances. However, as described before, the cluster structures exhibit important changes as described before.

The slight rise in λ with the surface coverage indicates an increasing tendency of large clusters to join with other large clusters. Short-range interactions must be responsible for this result since long-range ones are not present. Aggregation between uncovered sites on the particles cannot be responsible for this trend since this effect increases as the uncovered surface diminishes. The explanation could be based on the interaction between proteins of different particles. Despite the protein being globally discharged at the isolectric point, local charge fluctuations are present, which could be responsible for the unions between two large clusters when they are sufficiently close. Since large clusters bare large masses, a few unions must play a dominant role on the mean mass evolution. In order to confirm this mechanism, the aggregation rate constants were determined from the behaviors at shorter times.

The characteristic aggregation time, $t_c = 2/c_0 k_s$, was determined, and the aggregation constant for dimer formation calculated. Equation (6) obtains the characteristic aggregation time once d_f and λ are known. Figure 10 plots the aggregation constant k_s against the BSA-*m* and BSA-*p* covering. Within the range 0–50 % no important variations have to be pointed out. This result was expected since the high salt concentration and the protein isoelectric point guarantee diffusion conditions. In addition, the steric term, which reduces the collision efficiency, does not dominate due to the low protein coverage. Thus, the aggregation kinetics is protein independent. However, for 75% an important reduction is shown, and the system becomes completely stable at 100% coverage. Despite the diffusion condition which guarantees particle approximation, the binding forces (necessary for cluster formation) cannot act because of the presence of steric stabilizing forces. This mechanism is independent of

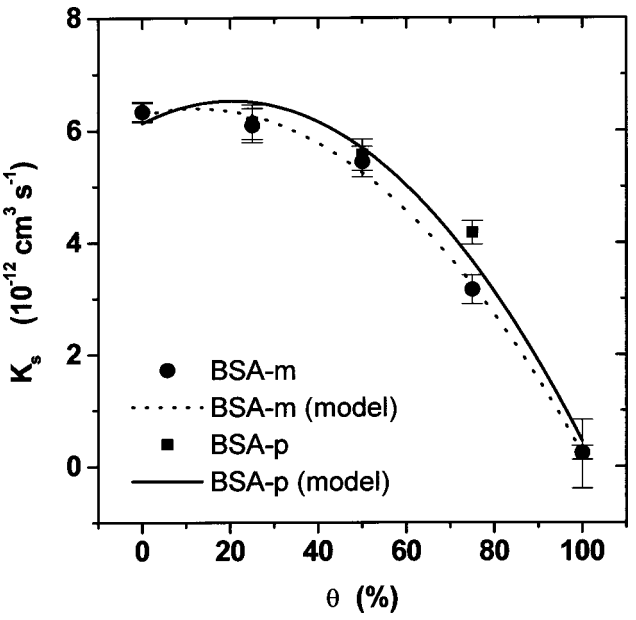

FIG. 10. Aggregation rate constant for dimmer formation at different surface coverage. Symbols correspond to monomeric and polymeric adsorbed BSA. Lines are the best fit to the model. The rate constants for the three contributions included in the model are summarized in Table I.

the size of the adsorbed molecules, once guaranteed that the binding forces cannot act. Figure 10 shows no relevant differences when polymeric protein is employed instead of the monomeric one, thus confirming that point.

Three possible aggregation mechanisms can be distinguished for molecule coverage particles. (a) *Surface-surface aggregation:* the collision of two uncovered sites on the surfaces occur. This process corresponds to the aggregation of bare particles, with k_{ss} being the rate constant. (b) *Protein-protein aggregation:* the collision of two protein patches occurs, being the aggregation rate is k_{pp}. (c) *Protein-surface aggregation:* bindings of uncovered sites on one particle with a covered part on another particle occur, forming bridges of macromolecules between particles. This reaction is characterized by k_{ps}.

Several theoretical models have been developed to explain the relation between the aggregation rate and the degree of coverage. La Mer [23] considered only bridging aggregation, assuming that the particle collision is completely controlled by particle diffusion, with binding probability equal to one. For pure bridging flocculation, k_s must be proportional to the number of free sites of protein on each particle θ and the number of occupied sites $(1-\theta)$, on the other. Therefore, $k_s \propto \theta(1-\theta)$. This relationship implies a maximum aggregation at half surface coverage and no flocculation at all for uncovered and totally covered particles.

TABLE I. Dimmer formation rate constants for surface-surface (k_{ss}), protein-protein (k_{pp}), and protein-surface aggregation (k_{ps}) from the aggregation model fitting.

Protein	k_{ss} $(10^{-12}$ cm^3 s$^{-1})$	k_{pp} $(10^{-12}$ cm^3 s$^{-1})$	k_{ps} $(10^{-12}$ cm^3 s$^{-1})$
BSA-*m*	6.1 ± 0.5	0.5 ± 0.4	8.1 ± 0.8
BSA-*p*	6.3 ± 0.2	0.2 ± 0.1	7.2 ± 0.3

The rest of the aggregation mechanisms are included in extended models [24–28]. Schmitt *et al.* consider one collision probability for each aggregation mechanism. The total rate of aggregation is obtained by adding all contributions up:

$$k_s = k_{ss}(1-\theta)^2 + k_{pp}\theta^2 + 2k_{ps}\theta(1-\theta). \tag{8}$$

The factor 2 describes bindings of covered and uncovered sites between two particles and its symmetrical case.

This relationship allows quantifying the contribution of the different aggregation mechanisms by plotting the rate of aggregation against the surface coverage (Fig. 10). The experimental rates of aggregation are two times higher than the La Mer model prediction. On the other hand, they lie very close to the value for diffusion-limited aggregation, 6×10^{-12} cm^3 s^{-1}, which indicates that all collisions for the surface-surface, protein-surface, and protein-protein aggregation mechanisms are effective. In the fitting procedure, the rate of aggregation for the surface-surface mechanism k_{ss} was set as the experimental rate of aggregation at $\theta=0$. The best fit is also shown in the Fig. 10 and the rates of aggregation are given in Table I. The results indicate that protein-protein coagulation does not play an important role, although it could be responsible for the slight trend of λ in Fig. 9. The protein-surface aggregation is then the predominant mechanism. This is responsible for the absence of aggregation at 100% coverage. The surface-surface mechanism is also dominant but becomes apparent just at low surface coverage. Because the experiments pH coincides with the protein isoelectric point, the BSA molecules do not alter the net charge of the colloidal particles. Thus, it is not surprising that the rate of aggregation for bridging flocculation is not far from surface-surface aggregation value.

ACKNOWLEDGMENTS

Financial support by Ministerio de Ciencia y Tecnología, projects MAT2000-1550-C03-01, MAT2000-1550-C03-02, and MAT2000-1550-C03-03 is acknowledged. We thank Dr. Manuel Quesada for kindly supplying the polystyrene particles. The Junta de Extremadura–Cousejería de Educación, Ciencia y Tecnología, as well as Foudo Social Europeo, are also acknowledged.

[1] H. Y. Lin, H. M. Lindsay, D. A. Weitz, R. C. Ball, R. Klein, and P. Meakin, Nature (London) **339**, 360 (1989).

[2] M. Carpineti and M. Giglio, Adv. Colloid Interface Sci. **56**, 73 (1993).

[3] M. L. Broide and R. J. Cohen, J. Colloid Interface Sci. **153**, 493 (1992).
[4] A. E. González, Phys. Rev. Lett. **71**, 2248 (1993).
[5] E. Dickinson and L. Eriksson, Adv. Colloid Interface Sci. **34**, 1 (1991).
[6] A. Fernández-Barbero, M. A. Cabrerizo-Vílchez, R. Martínez-García, and R. Hidalgo-Alvarez, Prog. Colloid Polym. Sci. **93**, 269 (1993).
[7] M. Tirado-Miranda, A. Schmitt, J. Callejas-Fernández, and A. Fernández-Barbero, Colloids Surf. **162**, 67 (2000).
[8] P. G. J. Van Dongen and M. H. Ernst, Phys. Rev. Lett. **54**, 1396 (1985).
[9] A. Fernández-Barbero, M. A. Cabrerizo-Vílchez, R. Martínez-García, and R. Hidalgo-Alvarez, Phys. Rev. E **53**, 4981 (1996).
[10] F. Gregory and I. Sheiham, Polym. J. (Tokyo) **6**, 7 (1974).
[11] J. K. G. Dhont, *An Introduction to Dynamics of Colloids* (Elsevier, Amsterdam, 1996).
[12] S. H. Chen and J. Texeira, Phys. Rev. Lett. **57**, 2583 (1986).
[13] M. V. Smoluchowski, Z. Phys. Chem. (Munich) **92**, 129 (1917).
[14] D. Asnaghi D, M. Carpineti, M. Giglio, and M. Sozzi, Phys. Rev. A **45**, 1018 (1992).
[15] D. E. J. Koppel, Chem. Phys. **57**, 4814 (1972).
[16] B. J. Olivier and C. M. Sorensen, J. Colloid Interface Sci. **134**, 139 (1990).
[17] M. Tirado-Miranda, A. Schmitt, J. Callejas-Fernández, and A. Fernández-Barbero, Prog. Colloid Polym. Sci. **104**, 138 (1997).
[18] H. Shirahama, K. Takeda, and T. Suzawa, J. Colloid Interface Sci. **109**, 552 (1986).
[19] J. Revilla, A. Elaissari, P. Carriere, and C. Pichot, J. Colloid Interface Sci. **180**, 405 (1996).
[20] J. P. Wilcoxon, J. E. Martin, and D. W. Shaefer, Phys. Rev. A **39**, 2675 (1989).
[21] G. Bolle, C. Cametti, and P. Tartaglia, Phys. Rev. A **35**, 837 (1987).
[22] B. Vincent, J. Edwards, S. Emment, and A. Jones, Colloids Surf. **18**, 261 (1986).
[23] V. K. La Mer, Discuss. Faraday Soc. **42**, 248 (1966).
[24] R. J. Hogg, J. Colloid Interface Sci. **102**, 232 (1984).
[25] S. G. Ash and E. J. Calyfield, J. Colloid Interface Sci. **55**, 245 (1976).
[26] B. M. Moudgil, B. D. Shah, and H. S. Soto, J. Colloid Interface Sci. **119**, 466 (1987).
[27] A. Molski, Colloid Polym. Sci. **267**, 371 (1989).
[28] A. Schmitt, A. Fernández-Barbero, M. A. Cabrerizo-Vílchez, and R. Hidalgo-Alvarez, Prog. Colloid Polym. Sci. **110**, 105 (1998).